Theoretical study of two expanded phases of crystalline germanium: clathrate-I and clathrate-II

1999 J. Phys.: Condens. Matter 11 6129

(http://iopscience.iop.org/0953-8984/11/32/305)

J. Phys.: Condens. Matter **11** (1999) 6129–6145. Printed in the UK PII: S0953-8984(99)04652-4

Theoretical study of two expanded phases of crystalline germanium: clathrate-I and clathrate-II

Jianjun Dong and Otto F Sankey

Department of Physics and Astronomy, and Materials Research Center, Arizona State University, Tempe, AZ 85287, USA

Received 28 May 1999

Abstract. We study two expanded phases of Ge crystals, type-I (Ge_{46}) and type-II (Ge_{136}) clathrates, using an *ab initio* density functional planewave pseudopotential method. The equation of state, electronic structure and vibrational modes have been determined. These expanded Ge phases are shown to be only slightly higher in energy than the diamond phase (0.05 eV/atom), and considerably lower in energy than the compressed β-tin phase by about 0.14 eV/atom. The electronic band-gaps of Ge clathrates are about 1.21 eV (type-I) and 0.75 eV (type-II) wider that band-gaps in the diamond phase. We have determined lattice vibrational modes and the frequencies of the Raman and infrared modes. The results of Ge clathrates are compared and contrasted with those of Si clathrates, where experiments are more numerous.

1. Introduction

Carbon, silicon and germanium have a similar valence electron configuration containing two s and two p electrons, and assemble in the diamond tetrahedrally bonded sp^3 solid as their ground-state crystal structure. Carbon is singular in that it takes on alternate forms with sp^2-bonds to produce graphite and icosahedral fullerene molecules. The icosahedral fullerene coalesce through van der Waals interactions to form open cage-based solids. Silicon and germanium too can form open cage-like solids involving icosahedra, but because of their inability to form sp^2-bonds, all cages are tightly joined with all atoms *4-connected* to retain sp^3-like bonding. The class of structures found experimentally are referred to as clathrates, because of their similarity to hydrate (ice) clathrates [1], which are H_2O framework solids with encapsulated guest impurities such as Cl_2. In hydrate clathrates there are four hydrogen bonds for each H_2O molecule; two hydrogen bonds of the oxygen with two neighbouring hydrogen atoms, and one hydrogen bond for each hydrogen atom with a neighbouring oxygen. This four-bonded motif is repeated in silica, where SiO_2 forms similar structures [2]. As early as 1965, scientists knew that silicon and germanium were capable of forming clathrate frameworks in the presence of guest metal atoms (such as Na and K) encapsulated into 'silicon cages' or 'germanium cages' [3–8]. No one, to our knowledge, has successfully produced a clathrate with no guest impurities. However, the guest fraction can, in some cases, be reduced to 1% or lower. The details of the clathrate-I and -II structures are given in section 3.

Silicon clathrates have been the most studied expanded semiconductor phase—several synthesis routes have been found and the structure analysed in detail. Semiconductor clathrate research has had a great increase in activity in the last six years, partially because of their similarities with fullerenes, but more importantly because of their expected new properties. Adams *et al* [9] reported their theoretical study on Si clathrates using a local-orbital tight-binding-like local density approximation (LDA) method. That study focused on pure silicon

0953-8984/99/326129+17$30.00

clathrates (i.e. the empty framework without metal guest atoms). They found that clathrate framework is approximately 0.07 eV/atom higher than the ground diamond-state phase, and that guest-free Si clathrates are semiconductors, whose band-gaps are about 0.7 eV wider than that of diamond phase. Other calculations have been performed on silicon clathrates by several theoretical groups [10–14].

The interest in semiconductor clathrates is not just in the semiconductor framework, but also in the control of the properties offered by the guests occupying the cages within the framework. The clathrate framework is open, and there are many possible guest atoms that can be inserted into the 'cages' and consequently alter the properties of the composite systems. This gives a material designer new 'knobs' by which the material properties can be tuned. An example of this is the recent discovery of superconductivity in $(Na, Ba)_x Si_{46}$, reported by Kawaji *et al* [15]. This novel discovery was unexpected since no superconductor had previously been found in a covalent sp^3 network. An earlier search for superconductivity was unsuccessful [16], since it appears that the element Ba plays a key role.

Germanium clathrate composites have drawn less attention than their silicon counterparts. A new motivation for their study has arisen because of their potential use as a thermoelectric material. A good thermoelectric material must have a high Seebeck coefficient S, high electrical conductivity σ, yet low thermal conductivity κ [17]. Currently, the bottleneck is to simultaneous satisfy the last two conditions because it requires that the solids are 'crystal-like' in term of electrical conductivity, but 'glass-like' in term of thermal conductivity. To overcome this dilemma, a new concept in designing thermoelectrics is to introduce 'rattling' vibrational modes to significantly reduce the thermal conductivity while the electrical conductivity is less effected [18]. Although the fundamental physics of these 'rattling' modes is not yet well understood, this concept has been successful within the skutterudites [19, 20]. Guided by these notions, Nolas *et al* [21] have shown that semiconducting Ge clathrates offer similar potential, and reported a remarkably low thermal conductivity in $Sr_8Ga_{16}Ge_{30}$. The structure of this solid is based on the framework type-I Ge clathrates (Ge_{46}), with all the 'cages' occupied by Sr atoms, and a fraction of the Ge sites are occupied by Ga atoms (a framework atom substituting for Ge). The guest Sr atoms (inside the cages) provide additional electrons to the electron deficient Ga atoms, to form a Sr^{2+} and $2Ga^{-}$ Zintl semiconducting compound. Likewise, the germanium clathrate-I framework has been shown to be the parent for a whole series of Zintl based compounds such as $K_8In_6Ge_{40}$ [22], $Ba_8M_8Ge_{38}$ (M = Zn, Cd), $Ba_8In_{16}Ge_{38}$ [23], $Rb_8Al_8Ge_{38}$ and $Cs_8Ga_8Ge_{38}$ [24].

The objective of the present study is to theoretically determined the basic properties of the 'pure' parent Ge framework clathrate materials including the vibrational spectrum which is important for characterization of the materials. In future work, we will study the effect of substitutional impurities and (caged) guest species. For both Ge_{46} (type-I) and Ge_{136} (type-II), we have determined the energetics of the framework, their equations of state and structural parameters, their electronic band-structure and their vibrational modes. We compare with the experiments where possible, and we compare and contrast with silicon clathrates where data is more plentiful. We report Raman and infrared (IR) vibrational modes, which can be used to compare and interpret future Raman and IR experiments. The vibrational modes are also key to understanding the thermal conductivity in these materials.

2. Computational methodology

The theoretical foundation of our calculations is LDA density functional theory (DFT) using a planewave basis and a pseudopotential. The method has been extensively tested on a wide variety of systems. The implementation we adopt here is particularly efficient. The calculations

were performed using the Vienna ab-initio simulation program (VASP) developed at the Institut für Theoretiche Physik of the Technische Universität Wien [25, 26] for large unit cells such as these, and uses an ultrasoft pseudopotential to eliminate core electrons in calculation [27, 28]. The electron exchange-correlation energy is approximated with the Ceperley–Alder functional [29]. We applied similar methods in a previous study of Si clathrates (Si_{136}) [13], and calculated structural and vibrational results are consistent with experiments [6, 30]. The effect of gradient corrections was examined in that work and were found to be minor, so we neglect them in this work. The energy cut-off of the planewave basis for Ge is chosen as 10.23 Ryd, and Brillouin zone integration is performed over a $2 \times 2 \times 2$ Monkhorst–Pack k-space grid.

Group theory is used to reduce the computation of the energy and forces during the structure optimization. To determine the optimized clathrate structures, we choose a fixed volume of the unit cell, then optimize the ionic positions through a conjugate gradient algorithm using atomic forces. This process is repeated for several unit cell volumes from which an equation of state and the global minimum energy is determined. Since the type-I and type-II clathrate structures are cubic (see section 3), optimizing the external lattice (in this case, a single lattice constant) is straight forward. The electronic states (band-structures) and vibrational modes are evaluated at the minimum energy configuration.

The calculation of lattice vibrational dispersion relations requires the dynamical matrix ($D(\vec{q})$), where $\vec{q}$ is is the phonon wavevector within the first Brillouin zone. Diagonalization of the dynamical matrix give the eigenvalues (squared frequencies) and eigenvectors. The calculation is performed in two steps. We start with a force free optimized unit cell with N atoms per cell. In the first step, we determine the $3N \times 3N$ Γ-point force constant matrix $\phi(\vec{q} = 0)$ by finite displacements of atoms within the large single unit cell of the material. A complete row of the matrix elements of $\phi(\vec{q} = 0)$ is determined from the forces generated on each atom when a single atom is displaced U_0 from its equilibrium position, and the force is divided by U_0. This procedure is exact in the harmonic approximation except for numerical errors. For a general structure, $3N$ such displacements must be made to capture the complete $\phi(\vec{q} = 0)$ matrix. Symmetry dramatically reduces this number and this is exploited. The symmetry unique displacements used for each of the two structures (clathrate-I and -II) will be described in section 3. Since Raman and IR modes only couple to near $\vec{q} = 0$ modes, this procedure generates these modes and the second step (described next) needed to determine the wavevector dependence is unnecessary for these modes.

In the second step, the dynamical matrix at non-zero $\vec{q}$ is obtained by introducing an extra approximation. This approximation assumes that atoms separated by a distance greater than third nearest neighbours (i.e. distances greater than 5 Å) have force constant matrix elements that have fallen to zero in real space. This 'distant force constant truncation' assumption allows us to obtain approximately the real space force constant matrix elements from the $\phi(\vec{q} = 0)$ force constant matrix. Then, from the approximate real space force constant matrix we reconstruct an approximate matrix in reciprocal space $\phi(\vec{q})$. The transformation from real space to reciprocal space is accomplished by performing the appropriate lattice/basis sum with the appropriate $\vec{q}$ dependent phase factors. Consequently, only the dynamical matrix at the Γ point ($\vec{q} = 0$) is calculated in an 'exact' way, and vibrational modes at other wavevectors are approximated since distant neighbour force constants are neglected. In diamond phase Ge, this approximation effects the transverse acoustic (TA) modes most. The error due to this truncation of the real space force constant matrix can be reduced by calculating $\phi(\vec{q} = 0)$ for a larger (supercell) cell to increase the real space range before it is truncated. With current workstations, a $2 \times 2 \times 2$ supercell calculation of Ge clathrates involves nearly 400 atoms and it is computationally impractical for such a LDA planewave calculation, and offers little

benefit. There is no error in the Raman and IR modes since they are computed in the first step†.

The method just described assumes the harmonic approximation is valid and this needs to be carefully checked in methods which use finite displacements. A displaced atom generates forces and these forces are divided by the displacement magnitude U_0 to obtain a force constant. Clearly the atoms must be carefully relaxed to their zero force positions for the procedure to be accurate. Here we use a value of U_0 of 0.02 Å and find the frequencies change little when we slightly vary this value. In addition, we perform force calculation with both $+U_0$ and $-U_0$ and average the two resulting force constant matrices. Any odd-order anharmonicity then vanishes, leaving only fourth- or higher-order anharmonic errors.

Raman or IR techniques can probe the vibrational modes. The intensity of first-order Raman scattering is proportional to the square of the change of polarization of the system. In this study, we estimate the Raman scattering intensity based on a bond-polarizability model (BPM) [31]. In the BPM, the change of polarization of the system is approximated by a sum of the changes of all the individual bonds. Furthermore, the BPM describes the bond polarization in terms of polarization expansion coefficients along the bond direction and normal to the bond. Empirical fitting from experiments has been performed for simple (diamond) covalent systems like C, Si and Ge with success [31, 32]. In our recent study of Si clathrates, we found those parameters are not transferable to new geometries [13], and we modify them empirically‡. The intensities (but not frequencies) should therefore be considered to be only qualitative. In addition, the frequency-dependent polarizability is replaced by a constant polarizability, and thus there can be no laser frequency dependence predicted for the spectra in the BPM that we use here.

3. Results

3.1. Structure, equation of state and energetics

Type-I clathrates have the $Pm\bar{3}n$ (No 223) space group. The 46 Ge atoms in its simple cubic (SC) primitive unit cell are located at three distinct Wyckoff symmetry sites: 6*c*, 16*i* and 24*k*. The material is open since it is obtained by packing two 'small' 20-atom cages and six 'large' 24-atom cages together. The two non-framework symmetry sites, 2*a* and 6*d*, are the centres of the 'small cage' (pentagonal dodecahedron) and the 'large cage' (tetrakaidecahedron) respectively. These cage-centred sites are generally occupied with alkali or alkali-earth metal atoms in synthesized clathrate materials. We study here guest free clathrates and focus on the pure framework.

The face-centred cubic (FCC) type-II clathrates belong to the space group $Fd\bar{3}m$ (No 227). This can be written in terms of its primitive cell as Ge_{34} (34 atoms per primitive unit cell) or in terms of its conventional cubic cell as Ge_{136} (136 atoms per cubic cell). This structure is obtained by packing eight 'small' 20-atom cages and sixteen 'large' 28-atom cages together in the conventional unit cell. The framework of Ge_{136} has three Wyckoff sites which are 8*a*, 32*e* and 96*g*, and the centres of the 'small cage' (pentagonal dodecahedron) and the 'large cage' (hexakaidecahedron) are 8*b* and 16*c* respectively. Stereo pictures of the clathrate structures can be found in [7, 9].

† In reporting the Raman and IR modes in this work, we use the results computed exactly for the $\vec{q} = 0$ force constant matrix, and not the approximate values obtained by determine the short-ranged real-space force constant matrix and the transforming back to reciprocal space. If we use the approximate matrix at the $\vec{q} = 0$ point, a maximum error of 5 cm^{-1} is found.

‡ In this study, we use $\alpha_1/\alpha_q = -3$ and $\alpha_{25}/\alpha_q = -0.5$.

In both type-I and -II, each Ge is tetrahedrally bonded (with no dangling bonds), and one would expect the material to be a semiconductor. We first determine the optimized structural parameters (table 1) and equation of state, EoS (table 2). The comparable experimental data is provided when it is available [5, 6, 8]. The samples measured in these experiments contain guest metal atoms inside the cages. We find that the LDA calculated lattice constants of Ge clathrates are about 1.5% (type-I) and 2.3% (type-II) smaller that those measured in experiments. The lattice constant of the Ge diamond phase calculated with the same approximations is 5.636 Å, which is only 0.3% smaller than the experimental value of 5.652 Å. In a previous study of Si [13] similar results were found (lattice constants about 0.6% too small), and the effects of the generalized gradient approximation (GGA) were to expand the lattice about 1.5% over the LDA results. Although this level of agreement is quite satisfactory and typical of the LDA, it is curious the diamond phase has so little error while the clathrate phases have a larger error. Two possible reasons come to mind. First the band-gap of diamond Ge is incorrectly predicted in LDA (see below), which may manifest itself by enlarging the lattice slightly to give the smaller error compared to clathrate. A second reason is that the experiments for Ge contain alkali metals which may expand the lattice slightly, giving the appearance that our clathrate calculation have a larger 'error'.

Table 1. The LDA optimized structural parameters of the Ge clathrate framework. Experimental results are from [5, 6, 8].

	Lattice constant		Fractional internal coordinates		
	Theory	Exp	Symmetry site	Theory	Exp
Ge_{46}	10.50 Å	10.66 Å	6*c* $(\frac{1}{4}, 0, \frac{1}{2})$ etc		
Clathrate-I			16*i* (x_i, x_i, x_i) etc	$x_i = 0.1835$	$x_i = 0.184$
			24*k* $(0, y_k, z_k)$ etc	$y_k = 0.3079$, $z_k = 0.1170$	$y_k = 0.313$, $z_k = 0.120$
Ge_{136}	15.13 Å	15.48 Å	8*a* $(\frac{1}{8}, \frac{1}{8}, \frac{1}{8})$ etc		
(or Ge_{34})			32*e* (x_e, x_e, x_e) etc	$x_e = 0.2170$	$x_e = 0.2177$
Clathrate-II			96*g* (x_g, x_g, z_g) etc	$x_g = 0.1825$, $z_g = 0.3704$	$x_g = 0.1822$, $z_g = 0.3704$

Table 2. The parameters of a Birch–Murnaghan equation of state obtained from a fit of the LDA energy against volume curve. The framework was optimized at each volume. The parameter E_0 is the minimum energy (binding energy), V_0 is the minimum energy volume, K is the bulk modulus, and $K' = \mathrm{d}K/\mathrm{d}P$ the volume derivative of the bulk modulus.

Phase	E_0 (eV/atom)	V_0 (Å^3/atom)	K (GPa)	K'
Diamond	−5.172 (0.000)	22.38 (100%)	70.2	4.7
β-tin	−4.986 (+0.186)	18.11 (81%)	80.1	4.7
Ge_{46} (I)	−5.122 (+0.050)	25.21 (113%)	61.3	4.8
Ge_{136} (II)	−5.128 (+0.044)	25.48 (114%)	61.9	4.8

The optimized values of internal coordinates are shown in table 1. We first discuss the Ge_{46} structure. The Ge–Ge bond-angles we obtain range from 104.9° to 124.7°. The ideal tetrahedral bond-angle in the diamond phase is 109.5°. At first sight, the fractional coordinates appear to be in close agreement with the experimental data for $K_{7.4}Ge_{45}$ [5]. (The Ge_{46} material is believed to have vacancies.) The agreement concerning Ge_{46} appears less satisfactory when these results are translated into bond-lengths. We find four distinct Ge–Ge bond-length which are 2.42 Å (bond-I), 2.43 Å (bond-II), 2.45 Å (bond-III) and 2.46 Å (bond-IV). The

four experimental bond-lengths are 2.42 Å (bond-III), 2.43 Å (bond-I), 2.50 Å (bond-II), and 2.57 Å (bond-IV). Theory thus predicts a much smaller spread in bond-lengths ($\delta d = 0.04$ Å) than does experiment ($\delta d = 0.17$ Å). We find this large difference to be somewhat alarming. We have further examined this difference by comparing the energies we obtain for (i) our optimized structure, and (ii) a structure with the experimental fractional coordinates given in table 1. This comparison was performed at the experimental lattice constant of 10.66 Å. We find an energy difference of 14.4 meV/atom (about 167 K in temperature units). This is a relatively large energy cost, being approximately one third of the energy cost of forming the clathrate phase over the diamond phase (see below). Theoretically then the wide range of bond-length noted in the experiments is unlikely. This suggest that (i) guests greatly alter the bond-lengths, (ii) vacancies or other defects exists at high concentrations altering the bond-lengths, (iii) the Reitveld refinements are inaccurate in determining the bond-lengths, or (iv) the LDA theoretical method is failing on this point. A final resolution of this point will have to await further work.

The early work of Cros *et al* [6] reported a lattice constant of 15.4 Å for Na_xGe_{136} samples. However, no detailed experimental data of the internal coordinates for the Ge_{136} type framework was available until very recently [8]. Bobev and Sevov [8] synthesized and characterized a fully-filled Ge clathrate, $Cs_8Na_{16}Ge_{136}$. They found a slightly larger lattice constant of 15.48 Å, and four distinct bond-lengths (2.4859 Å, 2.4881 Å, 2.4980 Å and 2.5033 Å). The spread in bond lengths is $\delta d = 0.017$ Å, much smaller than that of the data described earlier for Ge_{46} clathrates. The experimental and theoretical structure parameters are given in table 1. An LDA calculation shows that at the experimental lattice constant (15.48 Å), the energy difference between the structure with the experimental coordinates and the one with our optimized coordinates is negligibly small (1.3 meV/atom). Thus theory and experiment give consistent structure parameters in type-II Ge clathrates. The four bond-lengths found in our calculation are 2.415 Å, 2.4357 Å, 2.4362 Å and 2.461 Å, which gives a $\delta d = 0.046$ Å, a value similar to that obtained theoretically for Ge_{46} and *larger* than the experimental value.

We compute the EoS by fitting our calculated optimized energy at several different volumes to the Birch–Murnaghan equation. The equation for the energy against volume is [33]

$$E(V) = E_0 + \frac{9}{8} K\, V_0((V_0/V)^{2/3} - 1)^2 \left(1 + \left(\frac{4 - K'}{2}\right)\left(1 - \left(\frac{V_0}{V}\right)^{2/3}\right)\right).$$

and the parameters listed in table 2. There are four parameters; E_0 is the minimum energy (binding energy compared to free atoms), V_0 is the minimum energy volume, K is the bulk modulus, and $K' = \mathrm{d}K/\mathrm{d}P$ the volume derivative of the bulk modulus. Plots of the fitted EoS curves (at $T = 0$ K) of Ge clathrates, along with the ground state diamond phase and metallic β-tin phase, are shown in figure 1, where indeed diamond is the ground state. We have included the high-pressure β-tin phase which experimentally diamond transforms into near 8–10 GPa [34]. It is reduced in volume by approximately 19% and its energy is higher by about 0.186 eV/atom. The predicted phase transition pressure to the β-Sn phase 7.5 GPa.

The EoS of clathrate-I and -II are very close to each other. Compared with the diamond phase, their volumes are expanded by 13–14%. Their energies are close to diamond, being only 40–50 meV/atom higher. Since 50 meV is only 580 K in temperature units, the energy difference between Ge clathrates and Ge diamond is regarded as very small. The corresponding energy difference between diamond and clathrate phases in silicon was found to be about 70 meV/atom [13].

Obviously applying pressure to the diamond phase will not produce a phase transition to the expanded clathrate phases. As shown in figure 2, the free energy ($E + PV$, or Gibbs free

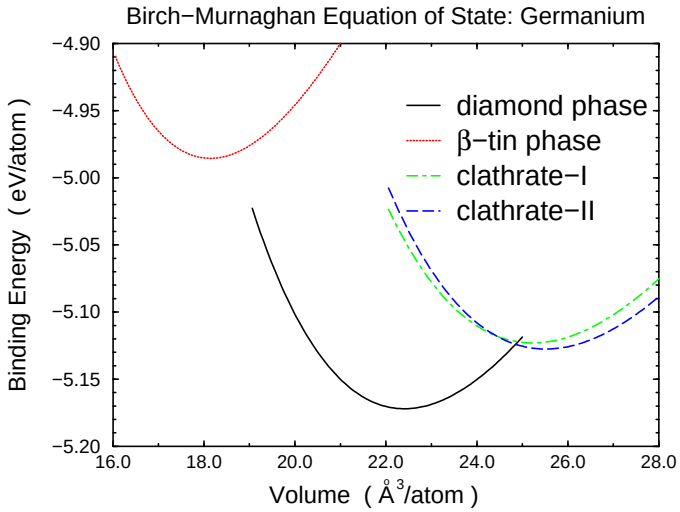

Figure 1. Equation of states (energy against volume) of four germanium phases: diamond, β-tin, clathrate-I (Ge_{46}) and clathrate-II (Ge_{136} or Ge_{34}). The LDA calculated data are fitted with the Birch–Murnaghan equation. Table 1 gives the parameters. In contrast to the high-pressure phases of Ge (such as β-Sn), clathrate phases are expanded phases whose EoS curves are located on the right of of the diamond phase.

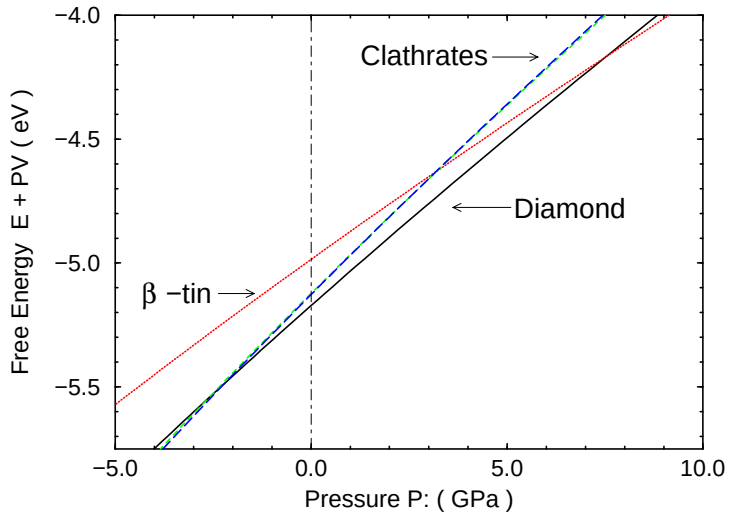

Figure 2. Free energy $E + pV$, of four germanium phases. Possible phase transitions are: diamond $\rightarrow$ β-tin at 7.5 GPa (exp 8–10 GPa); diamond $\rightarrow$ clathrates at about -2.2 to -2.4 GPa; clathrates $\rightarrow$ β-tin at 3.2 GPa.

energy at $T = 0$ K) of the diamond phase and clathrate phases are equal only for negative pressure (about -2.4 GPa for type-I and -2.2 GPa for type-II). However, phase transitions from clathrates to β-Sn are possible, and we find a critical pressure of about 3.2 GPa for both types of Ge clathrates. Other transitions may also occur such as that to the ST-12 phase. Early experiments by Bundy showed that Si clathrates 'collapsed' under pressure [35] to an undetermined, but complex, structure.

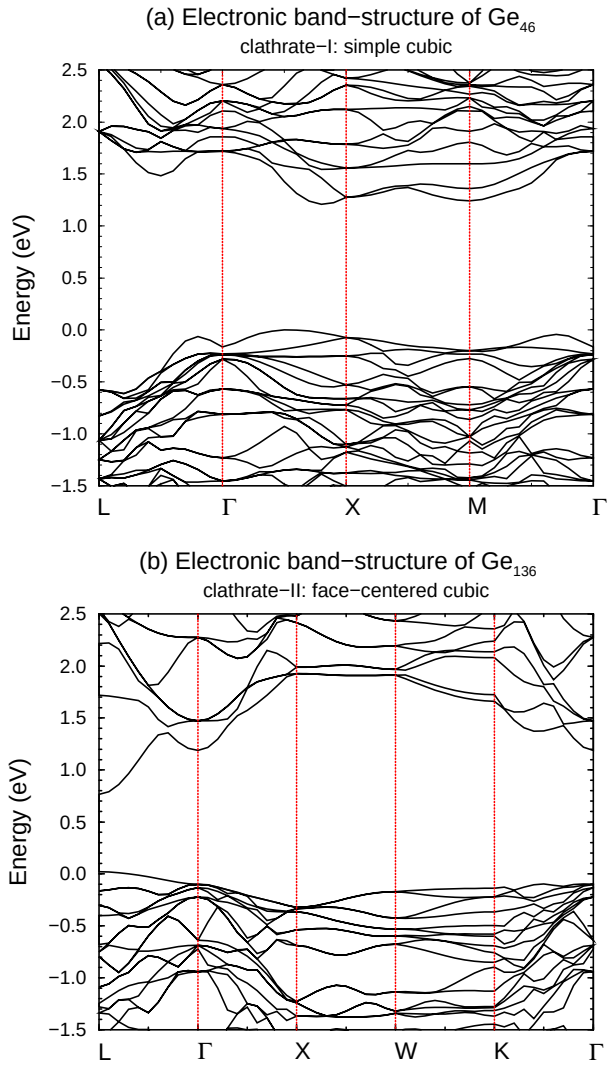

Figure 3. Electronic band-structure of: (a) Ge_{46} (clathrate-I); (b) Ge_{136} (clathrate-II); near the band-gap region. In units of $2\pi/a$, the k-points correspond to (a) $L = (\frac{1}{2}, \frac{1}{2}, \frac{1}{2})$, $\Gamma = (0, 0, 0)$, $X = (\frac{1}{2}, 0, 0)$, and $M = (\frac{1}{2}, \frac{1}{2}, 0)$; (b) $L = (\frac{1}{2}, \frac{1}{2}, \frac{1}{2})$, $\Gamma = (0, 0, 0)$, $X = (1, 0, 0)$, $W = (1, \frac{1}{2}, 0)$ and $K = (\frac{3}{2}, \frac{3}{2}, 0)$. Within the LDA, band-gaps are 0 eV (diamond, not shown), 1.21 eV (clathrate-I) and 0.75 eV (clathrate-II). Since the experimental band-gap of Ge diamond is 0.7 eV, we estimate that the LDA underestimates the size of gap by about 0.7 eV in the sp^3 bonded germanium solids. Using this estimation, the estimated gaps in Ge clathrates are 1.9 eV (type-I) and 1.45 eV (type-II).

3.2. Electronic band-structure

The LDA band-structure of diamond phase Ge leads to the well know failure of LDA—it predicts no band-gap, while of course, experimentally, diamond phase Ge is an indirect semiconductor of band-gap 0.7 eV. We performed the calculation for diamond phase Ge and find the top of valence and bottom of conduction band overlapping at the Γ-point. In other words, LDA underestimates band-gap in Ge diamond by at least 0.7 eV. To approximately correct for this shortcoming, we will add 0.7 eV (accompanied by a cautionary statement) to

our band-gap to obtain estimates of the true band-gaps for Ge clathrates. This assumes that the errors are relatively constant from one structure to the next—a reasonable assumption since the bonding is similar.

In figures 3(a) and (b), we show our calculated band-structure of Ge_{46} (type-I) and Ge_{136} (type-II) respectively. As in a previous study of Si clathrates [13], the electronic bands in Ge clathrates are fairly flat. We find band-gaps of 1.21 eV and 0.75 eV for clathrate-I and -II respectively. Adding the approximate 0.7 eV correction described earlier, we obtain estimates of 1.9 eV and 1.45 eV. For comparison, using the same theoretical technique for Si gives an estimate of 1.9 eV for both clathrate-I and -II [13]. The percentage increase in Ge clathrates is hence a bit larger.

The precise k-point to k-point transition of the minimum energy gap cannot accurately be determined because the bands are fairly flat, and small geometric changes and errors in the LDA (of GGA) may shuffle the ordering. In Ge_{46} (figure 3(a)), we find three distinct valence band maxima that are nearly degenerate. In addition, there are three local minima in the conduction bands. Within this particular LDA and structural model, the smallest energy gap is 1.21 eV and goes between k-points points that both lie along the Γ to X line. Since the k-point separation is small and the bands flat (particularly in the valence band region), we feel it best to conclude that Ge_{46} has a 'quasi-direct' band gap. The situation is clearer for Ge_{136} shown in figure 3(b). The FCC clathrate-II within the LDA is clearly a direct band-gap semiconductor of 0.75 eV at the L-point.

We compute the valence band electronic density of states of the three phase of Ge: diamond, clathrate-I and clathrate-II. The results are shown in figures 4(a), (b) and (c) respectively. The top of the valence bands is at 0 eV. We first observe that the valence band width for the clathrate phases is approximately 1 eV narrower than that for the diamond phase. Each density of states (DOS) shows three major structures which can be assigned (roughly) to an s-region, and sp-hybrid-region, and a p-region (from left to right) in the valence band region. The diamond phase clearly separates these phases, while the clathrate phases tend to meld these structures together. Mélinon *et al* [14] have described similar effects in the Si clathrate-II, and convincingly attribute these changes in the valence band DOS to the high density of five-fold rings. In a self-consistent planewave calculation (such as performed here) it is impossible to give a value of the valence band maximum on an *absolute* scale (e.g. to compare the valence band maximum of one phase relative to another or to vacuum). However, using a non-self-consistent tight-binding or local-orbital Harris functional, the valence band maximum can be placed on an absolute scale. We have done this using a local orbital Harris functional technique, and find that the valence band maximum moves down in energy by $\sim$2.1 eV in comparison with that of the diamond Ge phase [36]. Part of the reduction of the valence band width is due to the retreat of the band maximum, which also has the consequence of opening the band-gap. The narrowing in the width of valence bands by about 1 eV was also found in previous study of Si clathrates [13].

3.3. Lattice vibration and Raman spectra

We use symmetry to reduce the number of finite displacements needed to obtain the force constant matrix and the vibrational spectrum. In Ge_{46}, which has $Pm\bar{3}n$ symmetry, only six independent displacements need to be made. There must be a single displacement calculation of one atom at a 16i site, two orthogonal displacements for a single atom at a 6c site, and three orthogonal displacement calculations for a single atom at a 24k site. Group theory generates the remaining $(3 \times 46) - 6$ columns of the force constant ($\phi(\vec{q} = 0)$) matrix. Similarly, in Ge_{34}, only four displacements need be made instead of 102 ($=3 \times 34$) calculations.

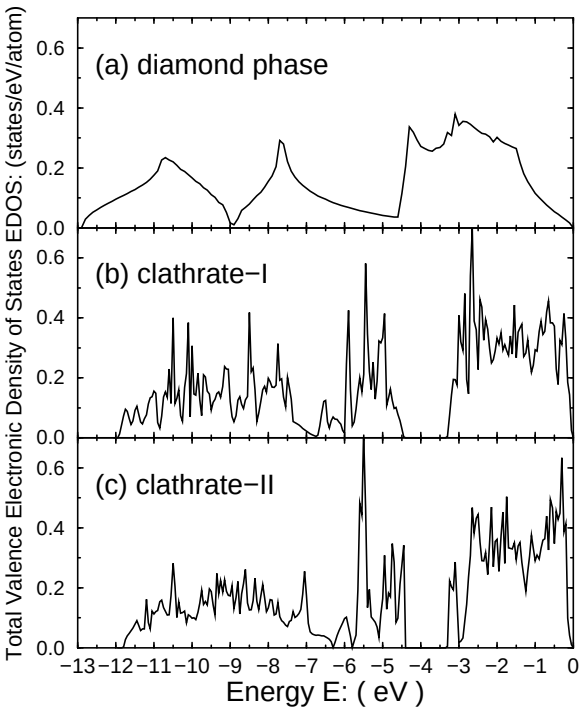

Figure 4. The total valence band electronic density of states (EDOS) of: (a) Ge diamond; (b) Ge_{46} (clathrate-I); and (c) Ge_{136} (clathrate-II). The valence band width for the clathrate phases is approximately 1 eV narrower than that for the diamond phase. The diamond phase clearly separates three regions (from left to right: s-region, sp-hybrid-region and a p-region), while the clathrate phases tend to meld these structures together. Note that the clathrates introduce a gap between the nominal sp-hybrid-region and the p-region.

The phonon dispersion curves for Ge clathrate-I and -II frameworks are shown in figures 5(a) and (b), and the phonon densities of states are in figure 6. Since these framework materials have large unit cells, the small Brillouin zone gives narrow bands. For both types of clathrates, there exist two high density of states regions—one is just above the acoustic branches (approximately from 50 cm^{-1} to 100 cm^{-1}), and the other is at the top of optical bands (approximately from 260 cm^{-1} to 285 cm^{-1}). As mentioned in section 2, the lowest TA modes ($\sim$0–30 cm^{-1}) are not as accurate as the other modes. The optical bands are generally flat, reminiscent of 'zone folding'. As a result, most optical modes, except a few within 100–150 cm^{-1} region, have very small group velocities ($d\omega(\vec{q})/d\vec{q}$). According to semi-classical heat transport theory [37], phonons with a small velocity transfer heat ineffectively. This suggests that even pure (empty cages) clathrates should have lower thermal conductivity compared with the diamond phase. Of course, such a comparison assumes identical phonon scattering mechanisms.

Optical modes are located from about 60 cm^{-1} up to about 285 cm^{-1} in both clathrate phases. For comparison, the highest optical mode in Ge diamond is 304 cm^{-1} (exp), and we calculate the frequency of Ge diamond to be 290 cm^{-1}. Thus our calculation shifts the highest mode frequency downward about 5 cm^{-1} compared to Ge diamond phase. In Si clathrates, a 30 cm^{-1} shift down from diamond phase in the highest optical modes was found [13, 30, 38].

Optical spectroscopy measurements, such as Raman or IR scattering, probe Γ point ($\vec{q} = 0$) phonon modes. To link our theoretical results with possible future experiments,

Table 3. Γ point ($\vec{q} = 0$) phonon modes of Ge_{46} (clathrate-I): frequencies and symmetry.

Frequency (cm^{-1})	Symmetry	Raman active	IR active
61.5	T_{2g}	✓	
62.8	T_{1g}		
67.1	E_g	✓	
68.7	T_{1u}		✓
71.3	T_{2u}		
74.4	T_{1g}		
77.3	T_{2g}	✓	
78.5	A_{2u}		
78.8	A_{2g}		
81.8	E_u		
83.3	T_{1g}		
88.9	T_{1u}		✓
89.0	T_{2g}	✓	
89.2	T_{1g}		
89.3	T_{2u}		
91.4	E_u		
92.8	T_{1u}		✓
131.5	E_g	✓	
138.0	T_{2u}		
138.6	A_{2g}		
169.8	E_g	✓	
172.2	T_{1u}		✓
175.7	T_{2g}	✓	
185.7	T_{2u}		
189.1	A_{1g}	✓	
190.1	A_{1u}		
206.2	T_{1g}		
211.7	T_{2u}		
215.1	T_{1u}		✓
218.1	A_{2g}		
222.8	A_{2u}		
234.9	T_{1u}		✓
235.2	T_{2g}	✓	
238.2	E_g	✓	
240.5	T_{1g}		
247.4	A_{1g}	✓	
257.7	T_{2u}		
263.4	T_{1u}		✓
268.3	E_g	✓	
270.7	T_{2u}		
272.2	T_{1g}		
272.2	T_{2g}	✓	
272.5	T_{1u}		✓
272.6	T_{2u}		
272.7	E_u		
274.6	T_{1u}		✓
275.0	E_u		
275.5	E_g	✓	
276.3	T_{2g}	✓	
276.9	A_{1u}		
277.8	T_{1g}		
278.2	T_{2g}	✓	

Table 3. (Continued)

Frequency (cm^{-1})	Symmetry	Raman active	IR active
278.7	E_g	✓	
279.0	A_{2g}		
281.6	T_{2u}		
282.4	A_{1g}	✓	

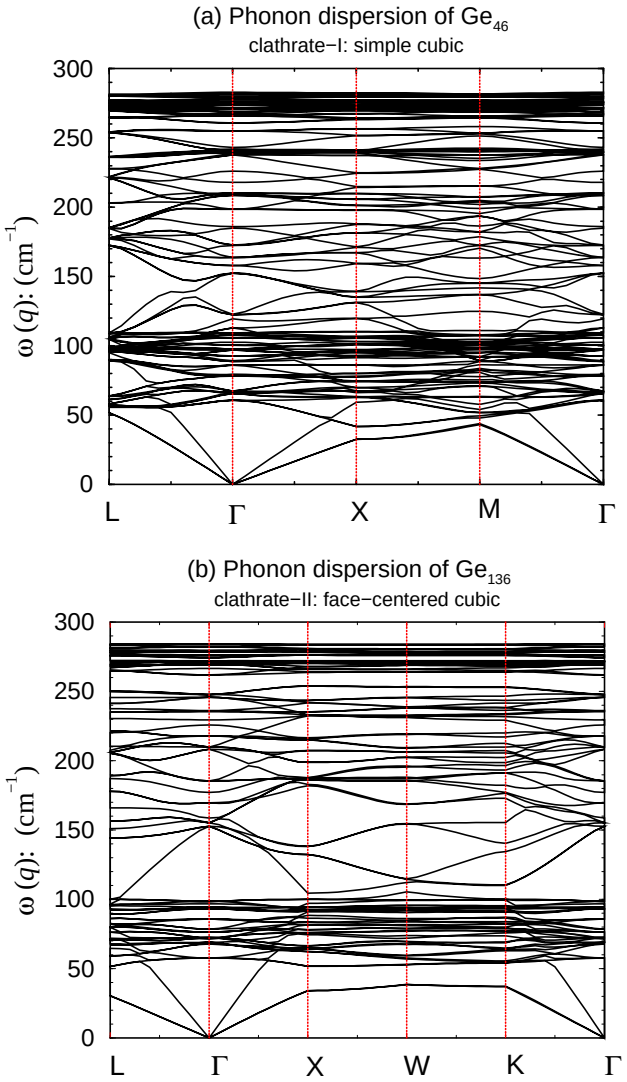

Figure 5. Phonon dispersion relations of Ge_{46} (clathrate-I) and Ge_{136} (clathrate-II), calculated approximately from the force constant matrix ϕ at the Γ point. The acoustic modes are located below 60 cm^{-1}.

we examine the frequencies and symmetry of Raman active or IR active modes [39] and the calculated results are listed in the tables 3 (Ge_{46}) and 4 (Ge_{136}). The mode frequencies listed are obtained directly from the finite displacement calculation, without the additional assumption of

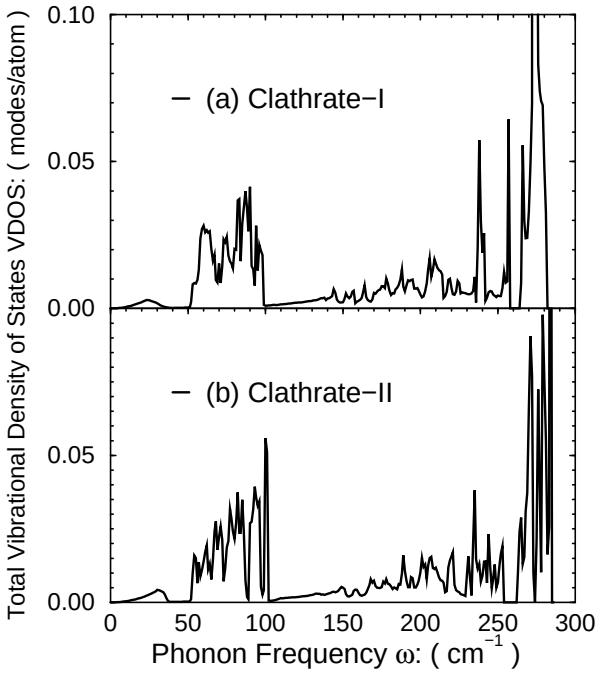

Figure 6. The total vibrational density of states (VDOS) of: (a) Ge_{46} (clathrate-I); and (b) Ge_{136} (clathrate-II). For both types of clathrates, there exist two high-density of states regions—one is just above the acoustic branches (approximately from 60 cm^{-1} to 100 cm^{-1}), and the other is at the top of the optical bands (approximately from 260 cm^{-1} to 285 cm^{-1}).

the distant force constant truncation approximation used to obtain the dispersion curves. Due to the degeneracy from structural symmetry, the 138 (3×46) Γ-point modes in Ge_{46} have only 57 distinctive frequencies ($3A_{1g} + 4A_{2g} + 7E_g + 8T_{1g} + 8T_{2g} + 2A_{1u} + 2A_{2u} + 4E_u + 10T_{1u} + 9T_{2u}$). Similarly, there are 42 frequencies ($3A_{1g} + 1A_{2g} + 4E_g + 5T_{1g} + 8T_{2g} + 1A_{1u} + 3A_{2u} + 4E_u + 8T_{1u} + 5T_{2u}$) for the 102 ($3 \times 34$) Γ phonon modes in Ge clathrate-II (Ge_{34}). Group theory [39] shows that there are 18 Raman allowed modes ($3A_{1g} + 7E_g + 8T_{2g}$), and 9 IR allowed modes ($9T_{1u}$, not including the T_{1u} zero-frequency translational modes) in Ge_{46} clathrate-I, and 15 Raman active modes ($3A_{1g} + 4E_g + 8T_{2g}$) and 7 IR active modes ($7T_{1u}$, not including the T_{1u} zero-frequency translational modes) in Ge_{34} clathrate-II.

The number of experimentally observed Raman or IR frequencies may be less than the number of active modes predicted by group theory since some modes have too small a scattering cross sections to be detected. To have a sense as to which modes we have calculated are 'invisible', we adopt a simple, empirical bond-polarizability model to estimate the Raman intensities (see section 2 for details). However, we emphasize that the intensity calculation is not quantitative. Previous work on Si clathrates has shown that the parameters for diamond phase are not transferable to clathrate phases. The parameters used in this study are chosen empirically (see second footnote on page 6132) using the rule found for Si [13]. We have calculated two types of polarization spectra: I_{xx} for parallel polarization (VV) and I_{xy} for crossed polarization (HV). The results are averaged over 4π solid angle to represent powder-like samples.

As shown in figure 7(a), the Raman spectra of Ge_{46} have five *major* peaks located at 67.1 cm^{-1}(E_g), 89.0 cm^{-1}(T_{2g}), 189.1 cm^{-1}(A_{1g}), 268.3 cm^{-1}(E_g) and 278.2 cm^{-1}(T_{2g}). Our calculated VV and HV spectra using the BPM confirm both E_g and T_{2g} modes are

Table 4. Γ point ($\vec{q} = 0$) phonon modes of Ge_{136} (clathrate-II): frequencies and symmetry.

Frequency (cm^{-1})	Symmetry	Raman active	IR active
54.1	T_{2g}	✓	
71.6	T_{1g}		
74.0	E_g	✓	
79.1	T_{1u}		✓
80.9	T_{2u}		
81.4	T_{1g}		
84.0	T_{2g}	✓	
87.6	E_u		
90.1	T_{1g}		
90.6	T_{2u}		
92.7	A_{2g}		
96.7	T_{1u}		✓
153.6	T_{1u}		✓
156.8	T_{2g}	✓	
162.0	A_{2u}		
169.6	E_u		
180.0	A_{1g}	✓	
187.5	T_{2g}	✓	
204.7	E_g	✓	
210.3	T_{2u}		
218.1	T_{1u}		✓
225.3	A_{2u}		
226.7	A_{1g}	✓	
233.8	T_{2g}	✓	
236.0	A_{2u}		
243.2	T_{1g}		
248.0	T_{1u}		✓
261.3	E_u		
268.2	T_{2u}		
269.3	T_{1u}		✓
270.0	A_{1g}	✓	
271.4	E_u		
273.0	E_g	✓	
273.6	T_{2g}	✓	
274.8	T_{1u}		✓
275.8	T_{2g}	✓	
278.9	T_{1g}		
281.4	T_{2g}	✓	
281.5	A_{1u}		
282.9	E_g	✓	
284.4	T_{2u}		

polarization insensitive, while A_{1g} modes are active only in parallel polarization. The VV spectra of Ge_{136} shown in figure 7(b) also shows five *major* peaks. Each of the first four peaks correspond to the individual Raman modes (54.1 cm^{-1}(T_{2g}), 74.0 cm^{-1}(E_g), 156.8 cm^{-1}(T_{2g}) and 180.0 cm^{-1}(A_{1g})), and the last peak is a combination of two modes (273.0 cm^{-1}(E_g) and 275.8 cm^{-1}(T_{2g})). There are also three *minor* peaks with frequencies of 84.0 cm^{-1}(T_{2g}), 226.7 cm^{-1}(A_{1g}) and 282.9 cm^{-1}(E_g). Again, A_{1g} modes are only active in the VV spectra.

Our previous calculation of Raman frequencies of (pure) Si_{136} are within a few per cent of reported Raman measurements performed with low Na concentration in Na_xSi_{136} samples

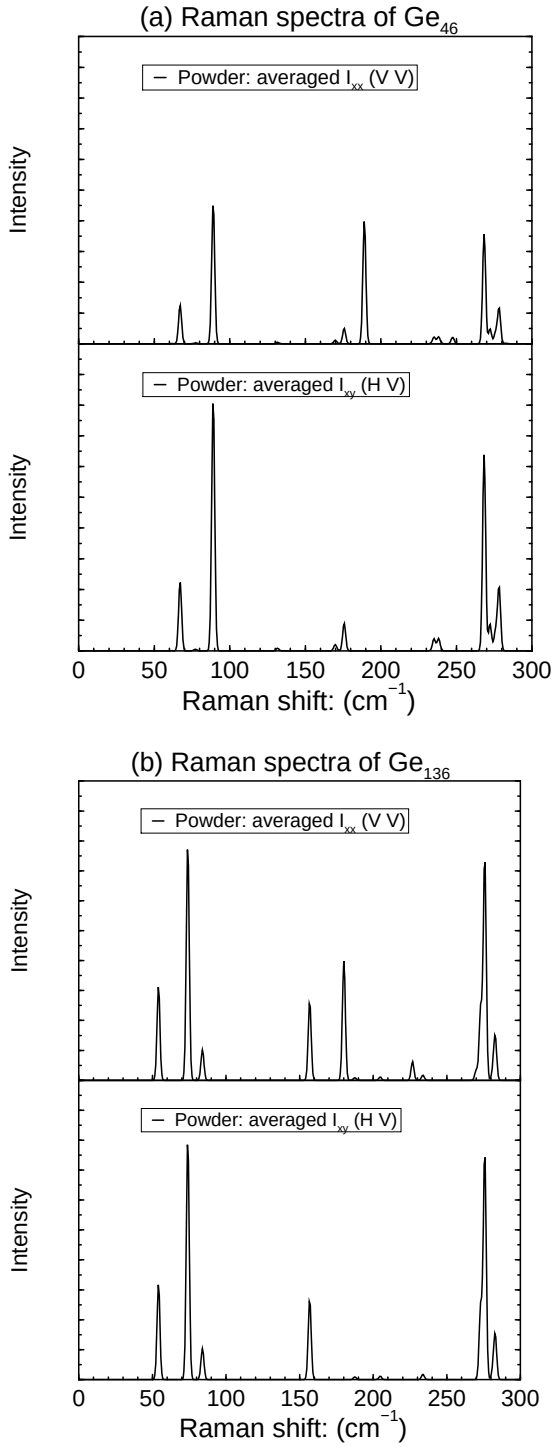

Figure 7. The calculated Raman spectra of (a) Ge_{46} (clathrate-I); and (b) Ge_{136} (clathrate-II). The relative intensity of first-order Raman scattering is computed using a bond-polarizability model, and the intensity is averaged over 4π solid angles appropriate to powder samples. The VV label is for parallel polarization, and the HV is the label for cross polarization.

[13, 30]. At the same time, a larger difference is found between the calculation of the Si_{46} phonon spectra and Raman experiments on high metal concentration Si_{46} samples, such as $(Na, Ba)_x Si_{46}$, Na_8Si_{46} and K_7Si_{46} [40]. Apparently, the metal–framework interaction is important for lattice vibration in these high metal concentration clathrates, and this likely applies to Ge_{46} as well.

4. Conclusions

We have determined the energetics, electronic structure, and vibrational modes of two germanium expanded phases—clathrate-I and clathrate-II. Comparing with the (ground state) diamond phase, the energies of Ge clathrates is only 0.04–0.05 eV/atom higher, while their volumes expand about 13–14%. Both type-I and type-II Ge clathrates are semiconductors, with LDA gaps of 1.21 eV and 0.75 eV respectively, and the true gaps (estimated correction of the LDA) are likely near 2 eV. The phonon dispersion curves show that the acoustic modes are limited to less than 60 cm^{-1} and most optical modes have small group velocity. We investigate phonon mode for IR and Raman experiments, and calculate the Raman spectra using a bond-polarizability model. We believe our results will be useful in interpreting future Raman or IR experiments and are obtained without any empirical fitting of the frequencies.

Acknowledgments

We thank the NSF (DMR-95-26274) and the NSF-ASU MRSEC (DMR-96-32635) for support. It is our pleasure to thank Ganesh Ramachandran, Professor Paul McMillan, Professor Jan Gryko, Professor Robert Marzke, Dr Alex Demkov and Dr George Nolas for many insightful discussions that we had in the course of this work.

References

[1] Claussen W F 1951 *J. Chem. Phys.* **19** 259
Claussen W F 1951 *J. Chem. Phys.* **19** 1425
Pauling L and Marsh R E 1952 *Proc. Natl Acad. Sci. USA* **36** 112
[2] Kamb B 1965 *Science* **145** 232
[3] Kasper J S, Hagenmuller P, Pouchard M and Cros C 1965 *Science* **150** 1713
[4] Cros C, Pouchard M and Hagenmuller P 1965 *C.R. Séances Acad. Sci. Ser.* A **260** 4764
[5] Cros C, Pouchard M, Hagenmuller P and Kasper J S 1968 *Bull. Soc. Chim. de France* **7** 2737
[6] Cros C, Pouchard M and Hagenmuller P 1970 *J. Solid State Chem.* **2** 570
Cros C, Pouchard M and Hagenmuller P 1971 *Bull. Soc. Chim. de France* **2** 379
[7] Gryko J, McMillan P F, Marzke R F, Dodokin A P, Demkov A A and Sankey O F 1998 *Phys. Rev.* B **57** 1
Ramachandran G K, Dong J, Diefenbacher J, Gryko J, Sankey O F, Marzke R F, O'Keeffe M and McMillan P F 1999 *J. Solid State Chem.* **145** in press
[8] Bobev S and Sevov S C 1999 *J. Am. Chem. Soc.* **121** 3795
[9] Adams G B, O'Keeffe M, Demkov A A, Sankey O F and Huang Y 1994 *Phys. Rev.* B **49** 8048
[10] Demkov A A, Sankey O F, Schmidt K E, Adams G B and O'Keeffe M 1994 *Phys. Rev.* B **50** 17 001
[11] Saito S and Oshiyama A 1995 *Phys. Rev.* B **51** R2628
[12] Smelyansky V I and Tse J S 1997 *Chem. Phys. Lett.* **264** 459
[13] Dong J, Sankey O F and Kern G 1999 *Phys. Rev.* B **60** 950
[14] Meĺinon P, Keǵhelian P, Blase X, LeBruse J, Perez A, Reny E, Cros C and Pouchard M 1998 *Phys. Rev.* B **58** 1
[15] Kawaji H, Horie H, Yamanaka S and Ishikawa M 1995 *Phys. Rev. Lett.* **74** 1427
[16] Roy S B, Sim K E and Caplin A D 1992 *Phil. Mag.* B **65** 1445
[17] Slack G A 1997 *Thermoelectric Materials—New Directions and Approaches* vol 478, ed T M Tritt *et al* (Pittsburgh, PA: Materials Research Society) p 47
[18] Slack G A 1995 *CRC Handbook of Thermoelectrics* ed D M Rowe (Boca Raton, FL: CRC) p 407

[19] Tritt T M 1999 *Science* **283** 804
[20] Mihaly L 1998 *Nature* **395** 839
Keppens V, Mandrus D, Sales B C, Chakoumakos B C, Dai P, Coldea R, Maple M B, Gajewski D A, Freeman E J and Bennigton S 1998 *Nature* **395** 876
[21] Nolas G S, Cohen J L, Slack G A and Schujman S B 1998 *Appl. Phys. Lett.* **73** 178
[22] Sportouch S, Tillard-Charbonnel M and Belin C 1994 *Z. Kristallogr.* **209** 841
[23] Kuhl B, Czybulka A and Schuster H-U 1995 *Z. anorg. allg. Chem.* **621** 1
[24] Kroner R, Peters K, von Schnering H G and Nesper R 1998 *Z. Kristallogr.* **213** 669
Kroner R, Peters K, von Schnering H G and Nesper R 1998 *Z. Kristallogr.* **213** 671
[25] Kresse G and Furthmüller J 1996 *Comput. Mater. Sci.* **6** 15
[26] Kresse G and Hafner J 1993 *Phys. Rev.* B **47** 558
Kresse G and Furthmüller J J 1996 *Phys. Rev.* B **55** 11 169
[27] Vanderbilt D 1990 *Phys. Rev.* B **41** 7892
Laasonen K, Car R, Lee C and Vanderbilt D 1991 *Phys. Rev.* B **43** 6796
[28] Kresse G and Hafner J 1994 *J. Phys.: Condens. Matter* **6** 8245
Kresse G and Hafner J 1993 *Phys. Rev.* B **48** 13 115
[29] Ceperley D M and Alder B J 1980 *Phys. Rev. Lett.* **45** 566
[30] Guyot Y, Champagnon B, Reny E, Cros C, Pouchard M, Melinon P, Perez A and Gregora I 1997 *Phys. Rev.* B **57** R9475
[31] Go S, Bltz H and Cardona M 1975 *Phys. Rev. Lett.* **34** 121
[32] Snoke D W and Cardona M 1993 *Solid State Commun.* **87** 121
[33] Birch F 1952 *J. Geophys. Res.* **57** 227
[34] Menoni C S, Hu J Z and Spain I 1986 *Phys. Rev.* B **34** 362
[35] Bundy F P and Kasper J S 1970 *High Temp.–High Press.* **2** 429
[36] Fuentes M and Sankey O F, unpublished
[37] Ashcroft N W and Mermin N D 1976 *Solid State Physics* (New York: Holt, Reinhart and Winston) p 500
[38] Demkov A A, Sankey O F, Daftuar S and Gryko J 1994 *Int. Conf. on Physics of Semiconductors* ed P J Lockwood (New Jersey: World Scientific) p 2205
[39] Fateley W G, Dollish F R, McDevitt N T and Bently F F 1972 *Infrared and Raman Selection Rules for Molecular and Lattice Vibrations: The Correlation Method* (New York: Wiley)
[40] Fang S L, Grigorian L, Eklund P C, Dresselhaus G, Dresselhaus M S, Kawaji H and Yamanaka S 1997 *Phys. Rev.* B **57** 7686